1994

Solitary wave dynamics of film flows

Liu Jun

Jerry P. Gollub
Haverford College

Solitary wave dynamics of film flows

Jun Liu and J. P. Gollub

Citation: Phys. Fluids **6**, 1702 (1994); doi: 10.1063/1.868232
View online: http://dx.doi.org/10.1063/1.868232
View Table of Contents: http://pof.aip.org/resource/1/PHFLE6/v6/i5
Published by the American Institute of Physics.

Solitary wave dynamics of film flows

Jun Liu and J. P. Gollub
Physics Department, Haverford College, Haverford, Pennsylvania 19041 and Physics Department, University of Pennsylvania, Philadelphia, Pennsylvania 19104

(Received 13 October 1993; accepted 31 January 1994)

The development and interaction of solitary wave pulses is critical to understanding wavy film flows on an inclined (or vertical) surface. Sufficiently far downstream, the wave structure consists of a generally irregular sequence of solitary waves independent of the conditions at the inlet. The velocity of periodic solitary waves is found to depend on their frequency and amplitude. Larger pulses travel faster; this property, plus a strong inelasticity, causes larger pulses to absorb others during interactions, leaving a nearly flat interface behind. These wave interactions lead to the production of solitary wave trains from periodic small amplitude waves. The spacings between solitary waves can be irregular for several different reasons, including the amplification of ambient noise, and the interaction process itself. On the other hand, this irregularity is suppressed by the addition of periodic forcing.

I. INTRODUCTION

Localized coherent structures, such as defects and solitary waves, often play an essential role in strongly nonlinear phenomena such as spatiotemporal chaos and even turbulent flows.[1–3] When a fluid system contains localized structures, complicated nonlinear phenomena may in some cases be described by the motions of these elementary elements, resulting in a dramatic reduction in the number of degrees of freedom.

Solitary waves (generally composed of a large maximum and several subsidiary maxima) occur commonly in the nonlinear behavior of liquid films flowing down an inclined (or vertical) plane. These solitary waves should not be confused with *solitons*, because the former are interacting and dissipative. Solitary waves in film flows were first noted in Kapitza's pioneering work[4] and were later studied by other researchers.[5–8] These flows also show a transition to turbulence, a process that may possibly be better understood through the dynamics of the solitary waves. (Other coherent structures such as turbulent spots[9] have also been observed in film flows.)

The purpose of this paper is to report an experimental study of the dynamics of two-dimensional solitary waves and their interactions, as part of an effort to understand more complex and disordered film flows. In next section, we discuss the literature relevant to this investigation. The experimental setup and measurement methods are briefly described in Sec. III. In Sec. IV, experimental results on periodic nonlinear waves and solitary waves are presented and compared with some theoretical work. We describe detailed studies of solitary wave interactions in Sec. V. Their collisions are found to be inelastic in the parameter range investigated here, so that large faster moving waves absorb smaller ones. This process provides a key to understanding the asymptotic development of wavy film flows. The generation of solitary waves through wave interactions is discussed in Sec. VI.

II. BACKGROUND

Flowing films are unstable to sufficiently long wavelength disturbances[10,11] when the Reynolds number is above its critical value $R_c=(5/4)\cot\beta$. Here, β is the inclination angle that the film plane makes with the horizontal; the Reynolds number $R=u_0h_0/\nu$ is based on the unperturbed film thickness h_0, the fluid velocity u_0 at the surface, and the kinematic viscosity ν. The Weber number $W=\gamma/(\rho h_0^2 g\sin\beta)$ is used to represent the effect of surface tension, where γ is the surface tension, ρ the liquid density, and g the gravitational acceleration. The initial instability is convective and the resulting waves are said to be noise sustained, i.e., sensitive to noise at the source.[12,13]

The nonlinear evolution of *periodically forced* waves depends strongly on the initial frequency f as determined by small perturbations near the inlet. Two-dimensional solitary waves appear at low frequency while saturated finite-amplitude waves occur at high frequency.[13,14] These periodic nonlinear waves are usually unstable to further two- and three-dimensional instabilities[15–18] and evolve into chaotic spatiotemporal patterns that involve solitary waves sufficiently far downstream.

Natural (unforced) waves due to ambient noise are selectively amplified as films flow downstream, and the average wavelength is initially close to the length scale determined by the most amplified wave number. However, saturated periodic waves do not appear without forcing because of nonlinear interactions and the convective character of the instability. Instead, fully developed three-dimensional waves are always irregular, and primarily consist of randomly distributed large solitary humps that control the hydrodynamic behavior and associated transfer processes.[19] Therefore, after sufficient nonlinear evolution, the flows are dominated by solitary waves *whether they are forced periodically or not.* This unique feature suggests that a coherent structure theory of the chaotic dynamics of film flows may have some merit.

Theoretical modeling of film flows was focused on linear and weakly nonlinear analyses before 1980.[7] Since then, researchers have made substantial progress on the strongly

 1070-6631/94/6(5)/1702/11/$6.00

nonlinear behavior, e.g., the evolution of solitary waves, by using dynamical systems theory and numerical simulations.[6,20–26] An evolution equation that can capture most of the nonlinear phenomena accurately is not available. However, a systematic long wave expansion yields a well-known equation due to Benney[27] that is valid for R close to R_c. It is successful in describing the initial evolution of nonlinear waves.[6,24,28] The dimensionless form of this equation is

$$h_t+2h^2h_x+\tfrac{2}{3}[\tfrac{4}{5}Rh^6h_x-h^3h_x\cot\beta+Wh^3h_{xxx}]_x=0, \tag{1}$$

to first order in the dimensionless wave number $\alpha=2\pi h_0/\lambda$, where λ is wavelength; the subscripts x and t denote partial derivatives. The length scale and time scale are h_0 and h_0/u_0, respectively. However, this equation can produce singularities in finite time,[6,24,29] and is of limited applicability.

The Kuramoto–Sivashinsky (KS) equation for film flows,[7,21]

$$\varphi_t+2\varphi_x+4\varphi\varphi_x+\tfrac{8}{15}(R-\tfrac{5}{4}\cot\beta)\varphi_{xx}+\tfrac{2}{3}W\varphi_{xxxx}=0, \tag{2}$$

has no singularities, but its applicability is limited to R very close to R_c and small wave amplitude $\varphi=h-1$. Chang, Demekhin, and Kopelevich[26] showed that model equations suitable for nonlinear waves at larger R have behavior similar to that of the KS equation. Therefore, the KS equation and certain extensions of it can provide a useful starting point for theoretical studies of film flows.

Chang *et al.*[26] investigated stationary traveling waves on vertical falling films using the KS equation for $R\to R_c=0$ and a boundary layer (BL) model for $R>0$. Assuming long wavelength and strong surface tension, the BL model[30] considerably simplifies the Navier–Stokes equations and boundary conditions into another group of equations that is appropriate for most fluids with $R<500$, and is more convenient to study numerically than the complete Navier–Stokes equations. As R approaches zero, stationary wave solutions of the BL equations collapse into those of the KS equation. Two nonlinear wave families (γ_1 and γ_2) were found. A wave denoted γ_1 has a smaller phase velocity than the linear one of the same wave number, while another denoted γ_2 travels faster. Solitary waves in the γ_2 family are called *positive* because of their *solitary humps*, but the γ_1 solitary waves are termed *negative* due to their *solitary dips*. (Pumir, Manneville, and Pomeau[6] also noted these two types of solitary waves.) The γ_1 family is so unstable for long wavelengths that it appears only at short wavelengths, while the γ_2 family predominates for long waves. These predictions have not been checked experimentally. On the other hand, computed solitary wave profiles compare well with those reported experimentally by previous authors.[26]

Solitary wave interactions in film flows are very different from the behavior of solitons in conservative systems because of dissipation. There have been several theoretical and numerical studies of solitary wave interactions in nonlinear models that are possibly related to film flows. Kawahara and Toh,[31] and later Elphick *et al.*[32] studied pulse interactions using an extended KS equation that includes a dispersive term φ_{xxx}. The equation is

$$\varphi_t+\varphi\varphi_x+\mu\varphi_{xx}+\delta\varphi_{xxx}+\vartheta\varphi_{xxxx}=0, \tag{3}$$

where $\mu>0$, $\delta>0$, and $\vartheta>0$ give the relative strengths of instability, dispersion, and dissipation, respectively. This equation contains the Burgers, KdV, and KS equations as special cases. These authors found that the complicated evolution exhibited by solutions of this equation can be qualitatively described by the weak interaction of pulses, each of which is a steady solution to Eq. (3). When the dispersion is strong, pulse interactions become repulsive, and the solutions tend to form stable lattices of pulses.[31]

In numerical simulations of films flowing down a vertical fiber,[33] Kerchman and Frenkel[34] found that the collision of two pulses, depending on various conditions, can be either an "elastic" rebound or an "inelastic" coalescence. A large pulse can grow by a cascade of coalescence when a modified Weber number S is larger than a threshold value which is close to that found experimentally by Quéré.[35] The evolution equation in this case is[33]

$$h_t+2h^2h_x+S[h^3(h_x+h_{xxx})]_x=0. \tag{4}$$

It differs from Eq. (1) for the vertical case in that the highest order nonlinearity is proportional to h^3 rather than h^6. However, this equation does not include dispersion effects.

There are few detailed experimental studies of solitary wave dynamics (other than wave profiles) in film flows. One exception is the work of Alekseenko, Nakoryakov, and Pokusaev.[14] They measured the wave velocity as a function of amplitude for various solitary waves on a vertically falling film.

III. EXPERIMENTAL METHODS

Our flow and measurement systems are briefly described as follows; a detailed description can be found in a previous paper.[13] The film plane is 200 cm long by 50 cm transverse to the flow; relatively small inclination angles from 4° to 10° are employed in this experiment. The entrance flow rate is perturbed at frequency f and amplitude A by applying small pressure variations to the entrance manifold. To suppress three-dimensional instability, aqueous solutions of glycerin (54% by weight) are used in this experiment; the kinematic viscosity and surface tension are 6.28 centistokes and 67 dyn/cm, respectively, at 22 °C. The working temperature varies by less than 0.4 °C in a few hours.

A fluorescence imaging method is used to measure the film thickness $h(x,y,t)$ in real time with a sensitivity of 8–10 μm.[13] For two-dimensional periodic waves, phase-sensitive averaging can be used to further improve the measurement sensitivity to 3–4 μm. We previously assumed a simple linear relation between the fluorescence intensity $I(x,y,t)$ and the film thickness $h(x,y,t)$ for films about 1 mm thick:

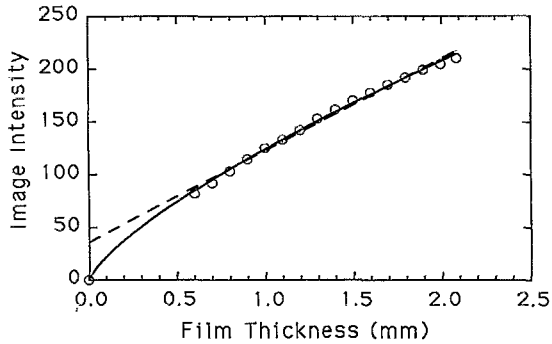

FIG. 1. Calibration of the fluorescence imaging method for glycerin–water solutions used in this experiment. The digitized fluorescence intensity is shown as a function of static film thickness. The solid curve is a fit to Eq. (6). The dashed line is a fit to Eq. (7).

$$I(x,y,t)=KI_0(x,y)h(x,y,t), \tag{5}$$

where $I_0(x,y)$ depends on the local illumination, and K is a constant. Our calibrations showed that this relation is accurate within 3% for pure water films from 0.5 to 1.5 mm thick and within 5% for glycerin–water films from 0.7 to 1.4 mm thick. Letting $\bar{I}(x,y)$ be the averaged fluorescence intensity of the unforced or static film, we have $h(x,y,t)/h_0=I(x,y,t)/\bar{I}(x,y)$ for small amplitude waves.

For the large amplitude waves investigated in this experiment, Eq. (5) is not sufficiently accurate. Careful calibrations over a larger range of film thickness showed that a power law relationship is satisfactory (Fig. 1):

$$I(x,y,t)=KI_0(x,y)[h(x,y,t)]^{\xi}, \tag{6}$$

where ξ is 0.87 for water and 0.74 for glycerin–water solutions. However, a linear approximation

$$I(x,y,t)=a(x,y)h(x,y,t)+b(x,y) \tag{7}$$

to this curve is usually sufficient, as indicated by the dashed line in Fig. 1. Here, $a(x,y)$ and $b(x,y)$ are fitting parameters; they depend on $I_0(x,y)$ and ξ.

We also measure the local wave slope $s(x_0,t)$ by laser beam deflection.[13] This signal is superior for the computation of spectra; its fractional sensitivity is about 5×10^{-5}, which corresponds typically to wave amplitudes of about 0.5 μm.

IV. EXPERIMENTAL RESULTS: NONLINEAR PERIODIC WAVES

The nonlinear development of forced periodic waves is strongly affected by their frequency. Solitary waves appear at low frequencies, and saturated finite-amplitude waves occur for high frequencies. For moderate $R(<70)$ and a wide range of frequencies, both types of waves can persist as quasistationary waves for a significant time even though they are unstable.[13,14] In this section we report experimental studies of these quasistationary waves which were made in order to test nonlinear theories and to investigate their further instabilities.

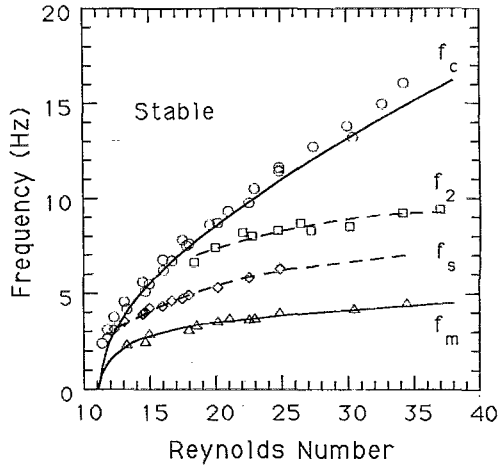

FIG. 2. Phase diagram in frequency f and Reynolds number R showing various regimes of linear stability, nonlinear evolution, and secondary instabilities. The inclination angle is $\beta=6.4°$, and aqueous solutions of glycerin (54% by weight) are used. See the text for a detailed explanation of the various theoretical lines and experimental measurements.

A. Phase diagram of two-dimensional waves

To provide a comprehensive picture of two-dimensional waves, we show in Fig. 2 a phase diagram in frequency and Reynolds number ($\beta=6.4°$) that pulls together results from our previous work.[13,15] The circles are measurements of the *neutral stability frequency* $f_c(R)$, below which the free surface is unstable. The upper solid line is calculated from linear stability theory. The triangles show measurements of the *maximum amplified frequency* $f_m(R)$, and the solid line through them is also the result of linear theory. We see that the linear stability theory is quite successful.

The bifurcation phase boundary denoted $f_s(R)$ separating two types of nonlinear evolution[13] is given by the diamonds in Fig. 2, with a smooth dashed line drawn through them. Between $f_s(R)$ and $f_c(R)$, we find *saturated* finite-amplitude waves with one maximum per period. Below $f_s(R)$, waves evolve into multipeaked waveforms, including solitary waves, by strongly nonlinear mechanisms.

Secondary instabilities: Another phase boundary $f_2(R)$ shown by squares in Fig. 2 separates the sideband and subharmonic two-dimensional secondary instabilities of periodic waves.[15] The sideband instability of the primary waves predominates above $f_2(R)$, and the subharmonic instability at frequencies below the boundary [and close to $f_m(R)$]. These secondary instabilities are convective and hence sensitive to noise. They initiate complicated coalescence and splitting processes of the wave fronts, and lead to spatiotemporal chaos downstream.[15]

We have investigated a range of small angles (4°–8°) and viscosities (2.8–6.5 cS). Varying these parameters always yields results that are qualitatively similar to those shown in Fig. 2 when R is close to R_c.

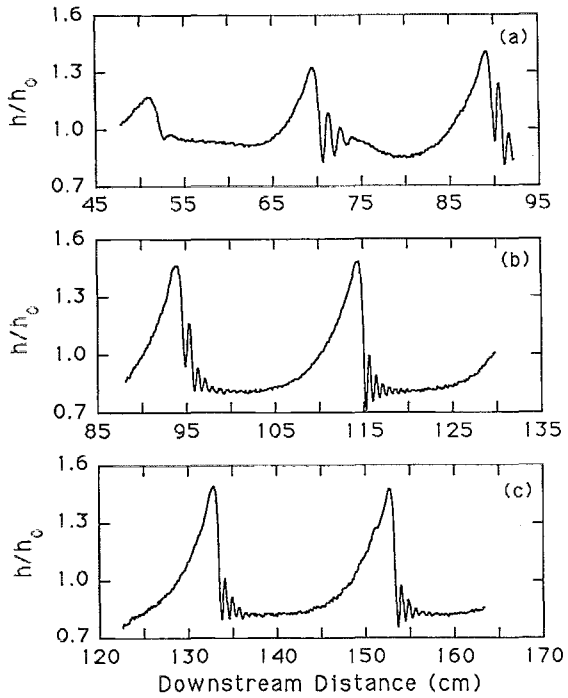

FIG. 3. The evolution of solitary waves forced at $f=1.5$ Hz with $\beta=6.4°$, $R=29$, and Weber number $W=35$. Three wave profiles are measured at increasing distances from the inlet to show the spatial evolution. Phase-sensitive averaging is employed here to reduce imaging noise.

B. Nonlinear evolution of periodic waves

Our previous studies of the nonlinear periodic waves[13] were limited to locating the bifurcation phase boundary $f_s(R)$ separating saturated single peaked waves from multipeaked solitary waves. In this subsection, we illustrate the subtle differences between various multipeaked waveforms and give examples of their evolution. (All conditions except the forcing frequency are kept constant in this subsection.)

An example of solitary wave evolution is given in Fig. 3, where the forcing frequency is $f=1.5$ Hz. Three wave profiles are taken at increasing distances from the source to show the spatial evolution. The phase-sensitive averaging method[13] is employed here to reduce the imaging noise. Initial sinusoidal waves near the inlet (not shown) become separated, developing steep fronts and stretched tails as the waves move downstream. Subsidiary wave fronts nucleate while primary peaks grow larger [Fig. 3(a)]. Further downstream, the primary waves gradually saturate [Fig. 3(b)]. Eventually, the solitary waves reach a stationary state in which successive pulses are nearly identical [Fig. 3(c)]. An image of the stationary solitary waves is shown in Fig. 4. The curvature of the wave fronts is due to boundary effects; our measurements are taken on the centerline. (We confirmed earlier[13] that the curvature does not affect quantitative agreement between stability theory and experiment for small amplitudes.)

We can project a solitary wave profile into phase space using spatial delay coordinates, as shown in Fig. 5. The resulting phase trajectory is qualitatively similar to a nearly

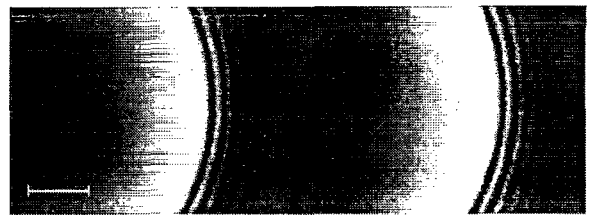

FIG. 4. A fluorescence image of stationary solitary waves with the same conditions as those in Fig. 3. The film flows from left to right. The left side of the image is at $x=123$ cm and the bar is 4 cm long.

homoclinic orbit as in the numerical work.[6,22] In this representation, the main wave is visible as a large loop extending far from the fixed point, while the precursor waves are shown as decaying orbits around this point. However, it is unclear whether this representation provides more than a qualitative method of visualization.

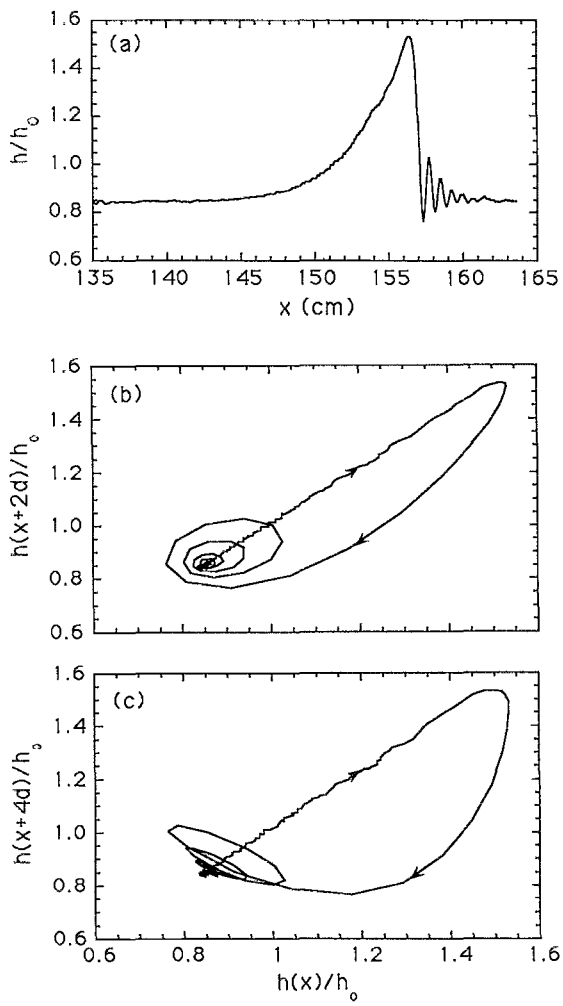

FIG. 5. Phase space representation of a solitary wave constructed using spatial delays: (a) solitary wave profile; ($f=1.25$ Hz, $R=27$, and $\beta=8°$). (b) The corresponding phase orbit obtained by plotting $h(x)$ vs $h(x+2d)$; (c) $h(x)$ vs $h(x+4d)$, where $d=0.16$ cm. The orbit resembles a nearly homoclinic orbit. The arrows on the trajectory show the direction in which x increases.

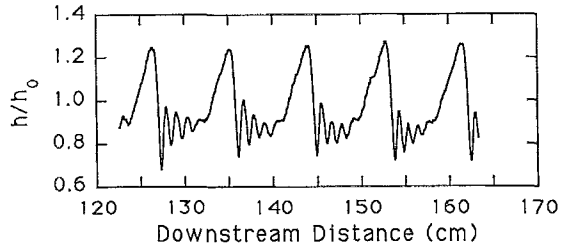

FIG. 6. Stationary approximate solitary waves forced at $f=3$ Hz ($\beta=6.4°$, $R=29$, and $W=35$); the waves interact significantly.

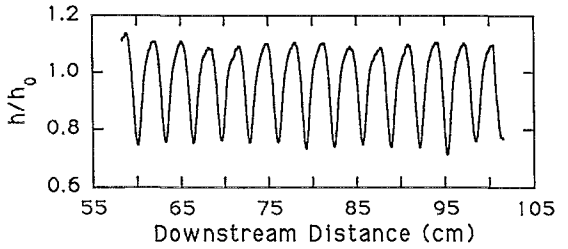

FIG. 8. Saturated single peaked waves forced at $f=7$ Hz with $\beta=6.4°$, $R=29$, and $W=35$. Waves of this type dominate at high forcing frequencies.

The generation of subsidiary waves may be viewed as a buckling of the surface as it is compressed by rapidly moving solitary humps. We find that the *subsidiary wavelength* of the solitary wave precursors is about half of the neutral wavelength predicted by linear stability theory based on the input Reynolds number.

When the frequency becomes larger, the primary wavefronts are closer together and the solitary waves cannot be clearly separated. Figure 6 shows a stationary wave of this type at $f=3$ Hz. The significant overlap of the front and tail may lead to strong interactions of these approximate solitary waves.

As the frequency is increased further in the multipeaked wave regime, the interactions become very pronounced and separate pulses are not formed. We show an example in Fig. 7 for a wave at $f=4.5$ Hz. When the subsidiary wave front is initially generated, a small depression appears on the primary peak and moves *faster* [Fig. 7(a)]. The velocity of the small depression is about 25.4 cm/s while the primary wave travels at 23.8 cm/s. The small depression passes the primary peak, and appears to form a subsidiary peak of that primary wavefront [Figs. 7(b) and 7(c)]. It is worth mentioning here that the waves are always periodic in time before losing their stability, even though they may appear nonperiodic in space.

For waves with frequencies above $f_s(R)$ (Fig. 2), there are no subsidiary maxima. Figure 8 gives an example at $f=7$ Hz. The wave profile becomes nearly sinusoidal and the saturated amplitude becomes smaller as f is increased. For very high frequency, the wave loses its stability before it reaches saturation.

C. Nonlinear velocity of periodic waves

In this subsection we present measurements of the linear and nonlinear wave velocities and compare them with theoretical predictions. The *linear velocity* is based on exponentially growing small waves.[13] Because periodic waves can reach quasistationary states over a large frequency range before losing their stability, we are able to determine the *nonlinear velocity* for these quasistationary waves. Waves at very low and very high frequencies are so unstable that their nonlinear velocity cannot be measured.

Figure 9 shows the linear velocity (squares) and nonlinear velocity (solid triangles) as functions of forcing fre-

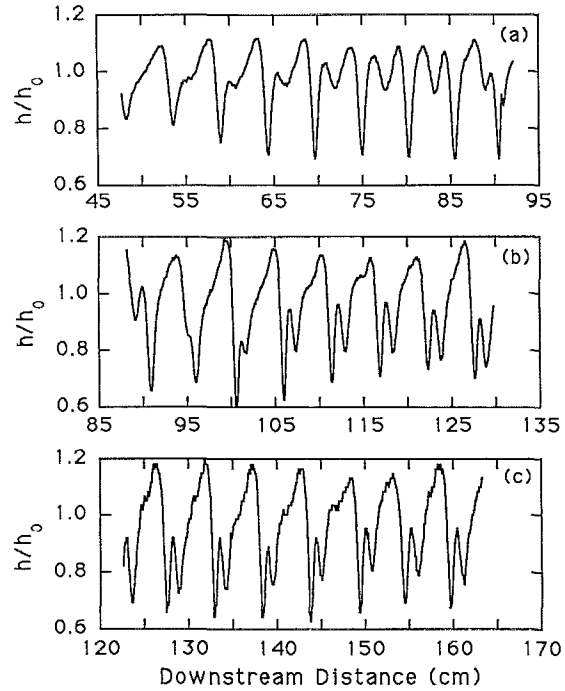

FIG. 7. The evolution of multipeaked waves forced at $f=4.5$ Hz with $\beta=6.4°$, $R=29$, and $W=35$. Faster moving subsidiary waves are observed in (a) and (b). [The phase-sensitive averaging method is not used for (c) because the secondary instability destroys the periodicity beyond $x=150$ cm.]

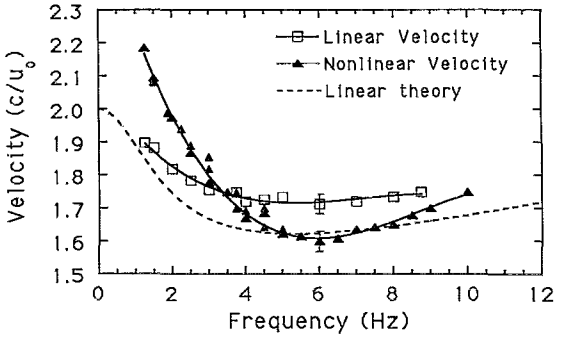

FIG. 9. The linear velocity (squares) and nonlinear velocity (solid triangles) as functions of forcing frequency ($R=29$, $\beta=6.4°$, and $W=35$ as for Figs. 3, 6–8). The solid lines are empirical fits to these velocities. The dashed curve is the prediction of linear stability theory. The velocities have been normalized by the surface velocity u_0 of the flat film.

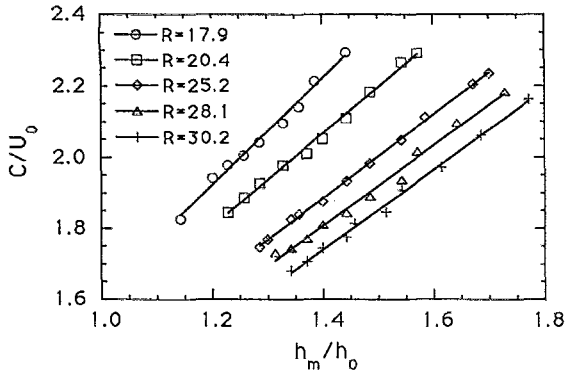

FIG. 10. The velocity of solitary waves as a function of their peak height for several R at $\beta=8°$. The wave velocity and peak height have been normalized by the surface velocity u_0 and thickness h_0 of a quiescent film.

quency. The velocities have been normalized by the surface velocity u_0 of the flat film. The solid lines are empirical fits to these velocities. The dashed line is the prediction of linear stability theory for small amplitude waves.[36] We see that the nonlinear velocity is *faster* than the linear one at low frequency, and *slower* at high frequency. The intersection of the linear and nonlinear velocities occurs at 3.4 Hz, which is smaller than the most unstable frequency $f_m \approx 4.1$ Hz. When the forcing frequency is close to the linear cutoff (neutral) frequency $f_c \approx 12.6$ Hz, the velocity difference between linear and nonlinear waves gradually becomes smaller.

The amplitude and velocity of periodic solitary waves are related to each other. We demonstrate this fact in Fig. 10, which shows the velocity of the periodic solitary (or nearly solitary) wave as a function of the peak height (h_m) for several Reynolds numbers, with an inclination angle $\beta=8°$. The wave velocity and peak height have been normalized by the surface velocity u_0 and thickness h_0 of a quiescent film. The wave velocity is proportional to the peak height. Larger amplitude waves are seen to move faster in each case. Similar results have been found for vertically falling films by Alekseenko, Nakoryakov, and Pokusaev.[14]

Weakly nonlinear theory[7,28,37] predicted for both inclined and vertical films that saturated waves close to the neutral curve travel more slowly than the linear waves while *saturated waves* somewhat farther from the neutral curve move faster. Because of the limitations of the long wave expansions[8,13,28] used in this theory, we cannot compare the predictions quantitatively with the experimental results. Our measurements agree qualitatively the predicted trends for waves close to the neutral curve. However, the measured intersection of the linear and nonlinear velocities occurs in the multipeaked region (see Fig. 1) instead of in the region of supercritically saturated waves predicted by the theory.

Our results on the velocity and the wave profiles (Secs. IV B and IV C) agree qualitatively with the predictions of Chang *et al.* for *vertically* falling films.[8,26] At a high frequency (or wave number), we see saturated waves which travel more slowly than the linear waves (Figs. 8 and 9). This behavior is similar to that of their γ_1 family of solutions (see Fig. 8 in Ref. 26). When the frequency is reduced through the threshold $f_s(R)$ we see multipeaked waves (Fig. 7). These initially have a form similar to the *negative* solitary waves [Fig. 7(a)] described by Chang *et al.* However, the negative solitary waves are unstable experimentally and lead to faster-moving subsidiary waves. If the frequency is small enough, positive solitary waves are dominant (Figs. 3 and 6). Their wave forms, the strongly increasing velocity at low frequencies, and the measured amplitude-velocity relation, are all similar to those of the γ_2 family of Chang *et al.*

V. INTERACTIONS OF SOLITARY WAVES

We explored the interactions of solitary waves systematically with the fluorescence imaging method and report the results in this section. The study of these interactions is fundamental to understanding the complex patterns produced by solitary wave trains. We first describe the interactions of a large solitary wave with a periodic train of smaller ones. We generate the periodic train by forcing at $f=2.5$ Hz, with $\beta=8°$ and $R=28$. Then we apply a pulse at the entrance to generate a larger solitary wave. The larger pulse moves faster than the others. It overtakes and absorbs the smaller ones in succession, as shown in Fig. 11. These *mergers* cause the incident pulse to grow significantly. This phenomenon is very different from the interactions of two solitons in the KdV equation where pulses "pass through" each other without losing their identity.[38]

The merging process is shown more clearly in the spatiotemporal data of Fig. 12 for $h(x,y,t)/h_0$, where initial periodic solitary waves are also forced at $f=2.5$ Hz. In these data, the time interval between successive profiles is 1/15 s. The incident pulse has a peak height $h/h_0 \approx 1.86$ and velocity $v \approx 34.5$ cm/s, while $h/h_0 \approx 1.55$ and $v \approx 28.5$ cm/s for the periodic waves. As the larger wave approaches and interacts with the smaller one, we see strong buckling phenomena between them, but there is no evident repulsion between them. Their interactions are inelastic in the sense that the waves merge. After the event, the peak height of the combined wave pulse is approximately 1.95 and the velocity has increased to about 36 cm/s. It is also worth noting that the interaction process leads to *wave suppression*: A very long flat interval (about 30 cm) is found between the combined pulse and the solitary wave behind it (not shown).

The same wave suppression effect occurs when a large solitary wave encounters well developed *natural* (unforced) waves. The large solitary wave absorbs all waves in front and leaves no trace of them behind it. In some cases the quiescent region is longer than 40 cm. We propose several possible reasons for this effect: (1) the smooth tail of a solitary wave may reduce the effective noise level in this region substantially; or (2) the growth rate of small perturbations may be lowered. The second of these seems more likely. We note that the thickness of the flat part in Fig. 12 is about $h=0.9h_0$, and its local Reynolds number is only $R=0.75R_0=24$. Both the growth rate and velocity of

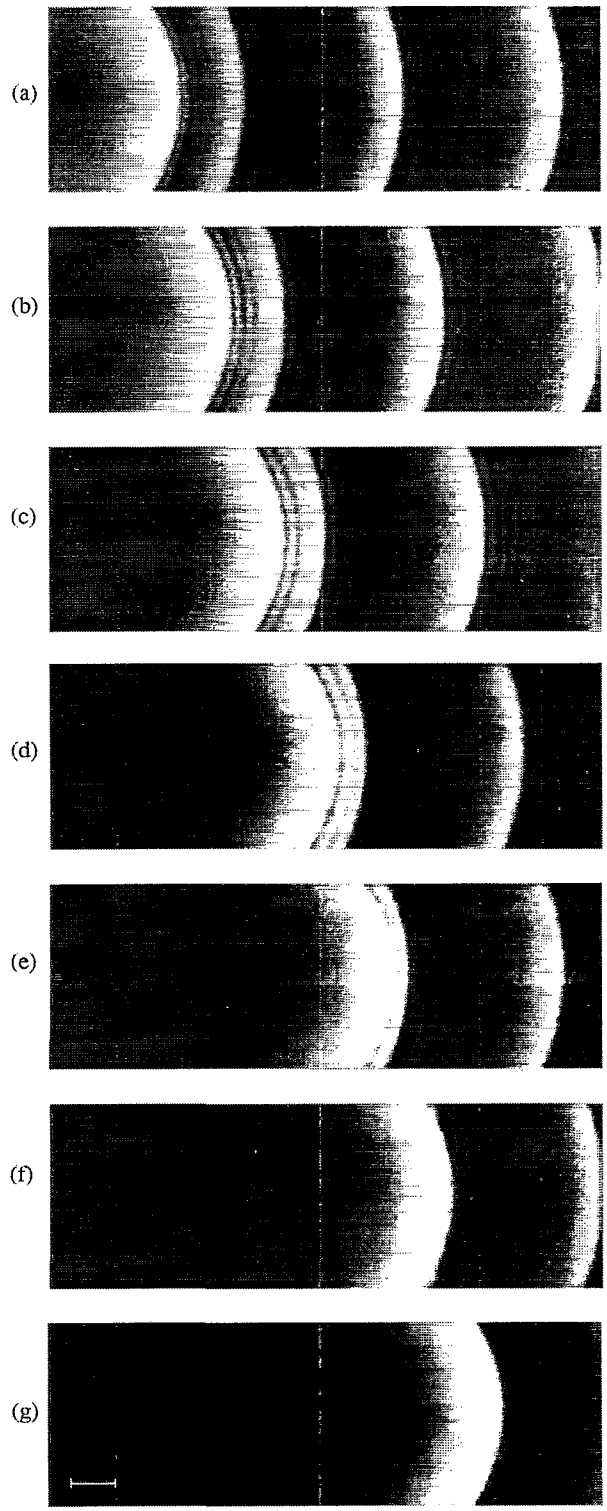

FIG. 11. Successive snapshots at time intervals of 0.2 s show the interaction of a large solitary wave with a small one. The large solitary wave overtakes and absorbs the small ones in succession. The left side of these images is 126 cm from the inlet, and the bar is 4 cm long. Here $\beta=8°$ and $R=28$.

small perturbations are therefore somewhat smaller. They may not have sufficient time to grow large enough to be seen before another solitary wave absorbs them.

The interactions discussed above are based on large

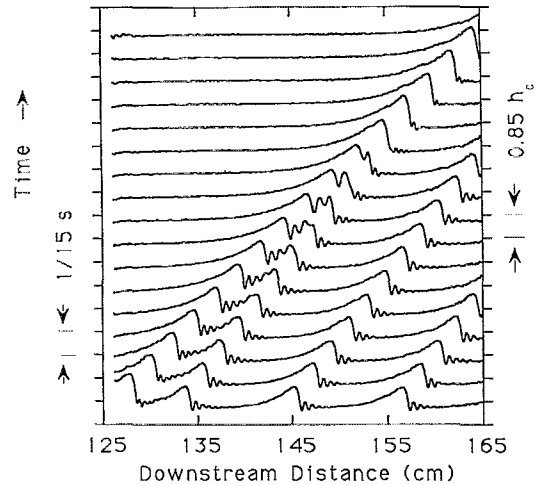

FIG. 12. Space–time evolution of the film thickness, showing the interaction of solitary waves. The wave profiles are shown at time intervals of 1/15 s; the amplitude scale is shown at the right. Here $\beta=8°$ and $R=32$.

amplitude differences. How do solitary waves with comparable amplitudes interact? In the KdV equation, solitons do not change after collision regardless of the amplitude difference, but the interaction processes vary with this parameter.[38] However, in a model for films flowing down a vertical fiber, Kerchman and Frenkel[34] found that both the pulse structures and the processes occurring during interaction change dramatically with the amplitude difference because of dissipation effects.

We find experimentally that the interaction of solitary waves with relatively small amplitude difference has the same result as for the case of large amplitude difference—*coalescence*. When a periodic solitary wave train is disturbed, a cascade of interactions can occur on a sufficiently long film plane, with the combined wave then overtaking and interacting with its neighbors. The interaction process can lead in this way to irregular wave trains downstream.

VI. GENERATION OF SOLITARY WAVES BY WAVE INTERACTION

Sufficiently far downstream, solitary wave trains develop *regardless* of initial perturbations.[5,13,14] Even though these waves can become three dimensional, they are closely related to the two-dimensional solitary waves at least for $R<200$ (see Fig. 9 in Ref. 13). The generation process of solitary waves is complicated. For low frequency periodic forcing, solitary waves result from the interaction of the forced wave and its harmonics.[24] (The usual three-wave interaction theory[39] is probably inadequate to deal with this phenomenon.)

For high frequency periodic forcing on the other hand, the process leading to solitary waves involves the convective secondary subharmonic and sideband instabilities[15] followed by wave interactions. In this section, we describe the development of two-dimensional solitary waves through such wave interactions. We impose two forcing frequencies to speed up the development of the solitary

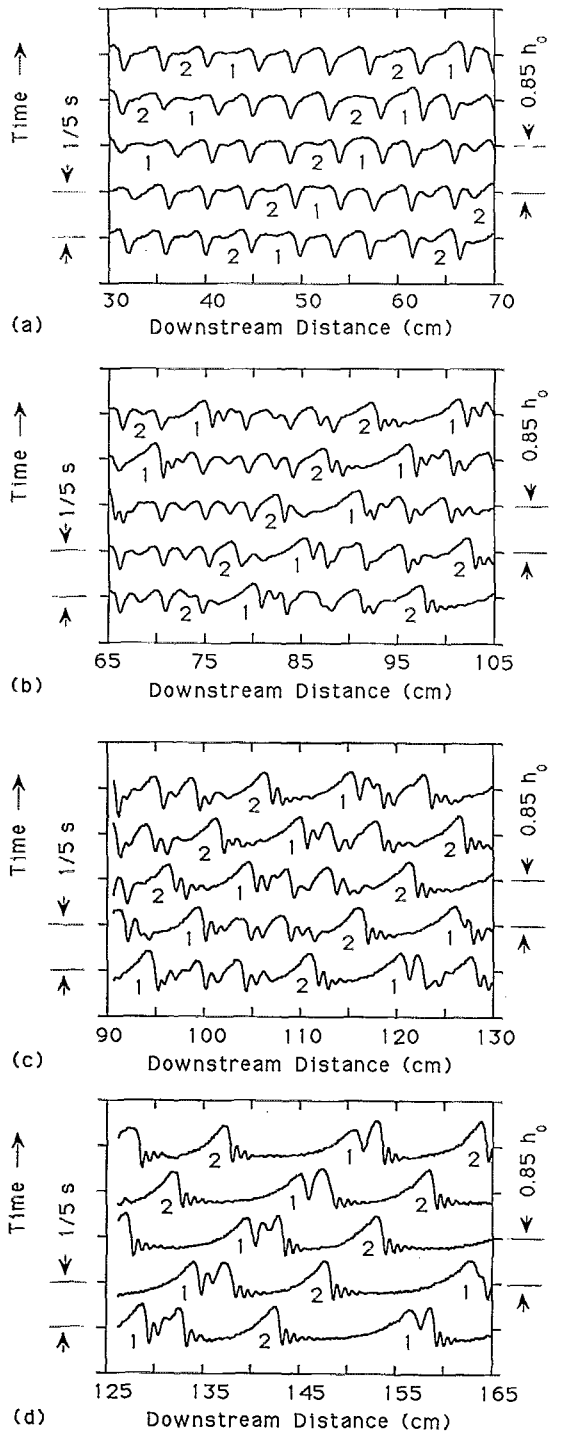

FIG. 13. Development of solitary wave trains through the interaction of waves forced at both 5 and 6 Hz. The four figures are taken at increasing distances from the source. The time intervals between successive wave profiles are 0.2 s. Since the waves are periodic in time (with period is 1 s), we can see the evolution by following the marked peaks from upstream to downstream locations. Because the camera had to be moved to obtain the four figures, the pulse labeled "2" in (d) is not literally the same pulse as the one with the same label in (a). ($R=27$, $W=33$, and $\beta=8°$.)

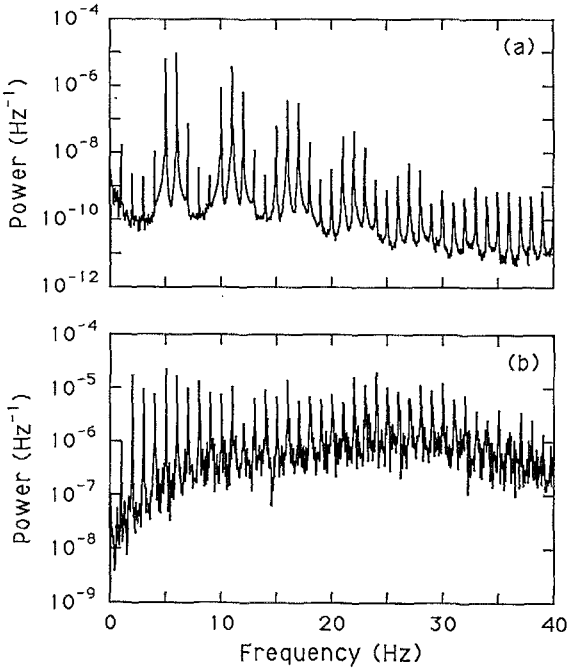

FIG. 14. The power spectra of local wave slope at (a) $x=23$ cm, and at (b) $x=136$ cm under the conditions of Fig. 13. The growth of broadband noise is evident.

waves, a useful expedient for experiments on a finite film plane. Finally, we discuss the effects of external noise on the spacing of pulses in solitary wave trains.

We choose two commensurate forcing frequencies of 5 and 6 Hz for $R=27$ and $\beta=8°$; they are close to $f_m=4.8$ Hz but do not separately generate periodic solitary waves in the 2 m length of our system. Their initial amplitudes are comparable. The nonlinear development is shown in the space–time diagrams of Fig. 13, which are taken at increasing distances from the source. Because the common period is 1 s, we show five snapshots of the wave profiles at 1/5 s intervals in each case.

To facilitate the reader's understanding of Fig. 13, we have marked two wave fronts that develop into solitary waves far downstream. In (a) we see that wavelengths are not uniform. The peaks with larger spacing ("1" and "2") grow and accelerate as they move downstream. They gradually absorb smaller peaks in front as they begin to develop into solitary waves with steep fronts and stretched tails [Fig. 13(b)]. Further downstream, some other fronts also develop into (nearly) solitary waves [Fig. 13(c)], but the larger faster-moving ones overtake and absorb them eventually, as shown in [(c), (d)]. Finally, in one period (1 s) we end up with only two solitary humps moving at roughly the same speed.

Power spectra computed from local slope measurements reveal that during this process all integer combinations of the two forcing frequencies are present (Fig. 14). The wave can be modeled as a periodic wave with an underlying broadband noise level that grows with distance downstream. The broadband component is mainly due to time variations in the subsidiary waves associated with the pulses. It is hard to determine whether this noise results from the interaction process or from amplification of ambient noise; both could be involved.

If the waves are driven by two *incommensurate* fre-

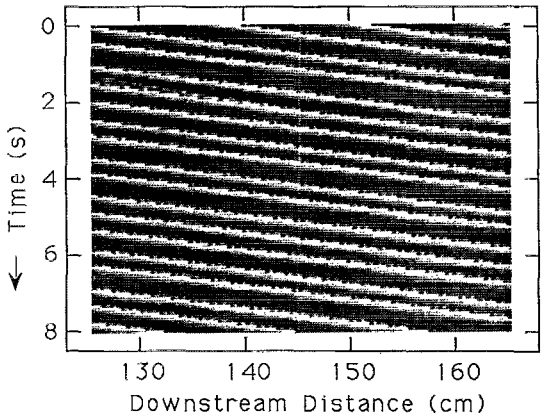

FIG. 15. Gray scale presentation of the spatiotemporal data of solitary wave trains forced at both 5 and 7.071 Hz. Each strip is a snapshot of the wave profile, and brightness corresponds to film thickness. The time interval is 1/15 s, and time increases downward. The wave spacings are irregular. ($R=27$, $W=33$ and $\beta=8°$.)

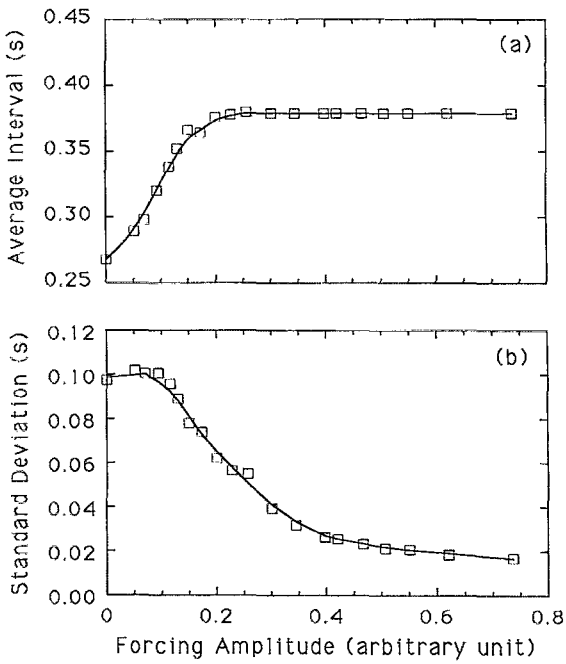

FIG. 16. The average time interval and the standard deviation of the interval as functions of the forcing amplitude. The data are taken at $x=149$ cm. Synchronization and suppression of irregularity are seen at large forcing amplitude. ($f=2.5$ Hz, $R=27$, $W=33$, and $\beta=8°$.)

quencies, the spacing of "final" solitary wave trains is clearly irregular. We give an example in Fig. 15, where the forcing frequencies are 5 and 7.071 Hz (approximately $5\sqrt{2}$ Hz). In this gray scale presentation of the spatiotemporal data, each horizontal strip is a snapshot of the wave profile, and brightness corresponds to film thickness. The time interval is 1/15 s. The spacings of the solitary waves are irregular, though the amplitudes are nearly identical. The velocities are also essentially identical, as may be seen from the fact that the world lines of the pulses are parallel. Therefore, their interactions will be very weak.

Natural (unforced) waves also evolve into solitary waves with fluctuating spacing because of the amplification of ambient noise. With the addition of periodic forcing at a *single* frequency, the natural irregularity is gradually suppressed. This effect is demonstrated in Fig. 16, where we show the average pulse interval and the standard deviation of the pulse interval at $x=149$ cm as functions of the forcing amplitude. Starting from natural (unforced) waves, we apply a weak forcing at $f=2.5$ Hz and gradually increase its amplitude from zero. At least 3000 solitary pulses are counted for each datum point shown. For natural waves, the time intervals are strongly fluctuating; the forcing is seen to synchronize the solitary waves even at large distances from the source.[40]

VII. DISCUSSION

A. Summary of the major results

We have made a systematic study of the velocities, development, and interactions of solitary waves on film flows with $15<R<50$ and $\beta=4°$–$10°$. They may be produced in many different ways: (a) by forcing at low frequencies, where the nonlinear interaction of forced frequency and its harmonics leads to the rapid development of localized pulses (Fig. 3); (b) by allowing high frequency periodic waves to evolve through secondary instabilities that produce *wavelength variations*,[15] with subsequent interaction and merging events leading to solitary waves; (c) by inducing wavelength variations artificially through multiple frequency forcing (as in Fig. 13); (d) or by the nonlinear evolution of natural waves, where the wavelength variations arise from ambient noise.

We first discussed the evolution and properties of stationary periodic solitary waves. We showed quantitatively how their velocity depends on both frequency and amplitude (Figs. 9 and 10). We have discussed these results in the context of the theoretical work of Chang *et al.*[26] and found qualitative agreement. The strong dependence of the solitary wave velocity on amplitude is particularly important in explaining the interactions of solitary waves.

The study of solitary wave interactions is critical to understanding the dynamics of film flows. Interactions are strongly *inelastic* in the sense that two interacting pulses *merge*: a large solitary wave overtakes and absorbs slower ones in front, leaving a long flat interface behind (Fig. 12). A cascade of interactions can occur on a sufficiently long film plane.

We studied the development of two-dimensional solitary wave trains through wave interactions. The growth of solitary waves is sensitive to the initial irregularity in the wave shape and size, with larger peaks growing faster [Figs. 13(a) and 13(b)]. The inelastic interaction of solitary waves results in a larger length scale as the waves evolve downstream (Fig. 13). We now understand that the irregularity of *spontaneous* solitary wave trains is primarily due to the initial wavelength variations caused by ambient noise. Under certain conditions, solitary waves can be synchronized over a long (but finite) distance by external forcing.

B. Concluding remarks

Solitary waves interact through the overlap of tails and oscillating fronts of successive pulses. Several authors[31,32] have studied pulse interactions within the framework of Eq. (3) using an effective-particle approach. They noted that bound states occur under certain conditions. In our experiments, we did not see significant repulsion or attraction (i.e., we saw almost no velocity changes) when two solitary pulses approach each other.

Dissipative collisions of solitary wave pulses have been noted by Kerchman and Frenkel[34] in a numerical simulation of films flowing down a vertical fiber, when their initial amplitude difference is large enough. Their evolution equation [Eq. (4)] includes stronger nonlinearity than does Eq. (3), but no dispersion.

Many of our observations remain to be quantitatively explained, and we hope that these experimental results may encourage further theoretical work. The relative importance of nonlinearity, dissipation, and dispersion in accounting for the observations merits special attention.

The inelasticity of wave interactions is responsible for the transition from small scale to large scale structures during flow downstream. Secondary instabilities[15] such as subharmonic instability *initiate* this transition, and then inelastic coalescence of waves with different velocities leads to a growth of scale. However, the mean spacing cannot increase indefinitely because the flat film between pulses will eventually become unstable. Some statistical equilibrium between coalescence events on the one hand, and nucleation events on the other, should be reached eventually. The nature of this final state, especially when it becomes three dimensional, remains to be explored.

ACKNOWLEDGMENTS

We appreciate helpful discussions with H.-C. Chang, W. S. Edwards, A. L. Frenkel, and P. Tabeling. We also thank B. J. Gluckman, D. P. Vallette, and J. Schneider for assistance.

This work was supported by the National Science Foundation under Grant No. CTS-9115005.

[1] D. J. Tritton, *Physical Fluid Dynamics* (Clarendon, Oxford, 1988).
[2] J. T. C. Liu, "Coherent structures in transitional and turbulent free shear flows," Ann. Rev. Fluid Mech. **21**, 285 (1989).
[3] M. C. Cross and P. C. Hohenberg, "Pattern formation outside of equilibrium," Rev. Mod. Phys. **65**, 851 (1993).
[4] P. L. Kapitza and S. P. Kapitza, "Wave flow of thin layers of a viscous fluid: III. experimental study of undulatory flow conditions," Zh. Exper. Teor. Fiz. **19**, 105 (1949). Also in *Collected Papers of P. L. Kapitza*, edited by D. Ter Haar (Pergamon, New York, 1965), Vol. 2, pp. 690–709.
[5] A. E. Dukler, "Characterization, effects and modeling of the wavy gas-liquid interface," in *Progress in Heat and Mass Transfer*, edited by G. Hetsroni, S. Sideman and J. P. Hartnets (Pergamon, New York, 1972), Vol. 6, pp. 207–234.
[6] A. Pumir, P. Manneville, and Y. Pomeau, "On solitary waves running down an inclined plane," J. Fluid Mech. **135**, 27 (1983).
[7] S. P. Lin and C. Y. Wang, "Modeling wavy film flows," in *Encyclopedia of Fluid Mechanics*, edited by N. P. Cheremisinoffs (Gulf, Houston, 1985), Vol. 1, pp. 931–951, and references therein.
[8] H.-C. Chang, "Wave evolution on a falling film," Annu. Rev. Fluid Mech. **26**, 103 (1994), and references therein.
[9] J. R. Bertschy, R. W. Chin, and F. H. Abernathy, "High-strain-rate free-surface boundary-layer flows," J. Fluid Mech. **126**, 443 (1983).
[10] T. B. Benjamin, "Wave formation in laminar flow down an inclined plane," J. Fluid Mech. **2**, 554 (1957).
[11] C. S. Yih, "Stability of liquid flow down an inclined plane," Phys. Fluids **6**, 321 (1963).
[12] R. J. Deissler, "External noise and the origin and dynamics of structure in convective unstable systems," J. Stat. Phys. **54**, 1459 (1989).
[13] J. Liu, J. D. Paul, and J. P. Gollub, "Measurements of the primary instabilities of film flows," J. Fluid Mech. **250**, 69 (1993).
[14] S. V. Alekseenko, V. Y. Nakoryakov, and B. G. Pokusaev, "Wave formation on a vertical falling liquid film," AIChE J. **31**, 1446 (1985).
[15] J. Liu and J. P. Gollub, "Onset of spatially chaotic waves on flowing films," Phys. Rev. Lett. **70**, 2289 (1993).
[16] J. Liu, J. D. Paul, E. Banilower, and J. P. Gollub, "Film flow instabilities and spatiotemporal dynamics," in *Proceedings of the First Experimental Chaos Conference*, edited by S. Vohra, M. Spano, M. Shlesinger, L. M. Pecora, and W. Dittos (World Scientific, Singapore, 1992), pp. 225–239.
[17] S. W. Joo and S. H. Davis, "Instabilities of three-dimensional viscous falling films," J. Fluid Mech. **242**, 529 (1992).
[18] H.-C. Chang, M. Cheng, E. A. Demekhin, and D. I. Kopelevich, "Secondary and tertiary excitation of three-dimensional patterns on a falling film," J. Fluid Mech. (in press, 1994).
[19] K. J. Chu and A. E. Dukler, "Statistical characteristics of thin wavy films, part III: structure of the large waves and their resistance to gas flow," AIChE J. **21**, 583 (1975).
[20] O. Y. Tsvelodub, "Stationary traveling waves on a film falling down an inclined plane," Izv. Akad. Nauk. SSSR, Mekh. Zhid. Gaza, No. 4, 142 (1980) [English translation: Fluid Dyn. **15**, 591 (1980)].
[21] G. I. Sivashinsky and D. M. Michelson, "On irregular wavy flow of a liquid film down a vertical plane," Progr. Theor. Phys. **63**, 2112 (1980).
[22] S. P. Lin and O. Suryadevara, "Solitary, periodic and chaotic waves in thin films," in *Transactions of the 2nd Army Conference on Applied Mathematics and Computing* (ARO Report 85-1, 1985), pp. 483–499.
[23] H.-C. Chang, "Onset of nonlinear waves on falling films," Phys. Fluids A **1**, 1314 (1989).
[24] S. W. Joo, S. H. Davis, and S. G. Bankoff, "Long-wave instabilities of heated falling films: two-dimensional theory of uniform layers," J. Fluid Mech. **230**, 117 (1991).
[25] Y. Y. Trifonov, "Steady-state traveling waves on the surface of a viscous liquid film falling down on vertical wires and tubes," AIChE J. **38**, 821 (1992).
[26] H.-C. Chang, E. A. Demekhin, and D. I. Kopelevich, "Nonlinear evolution of waves on a vertically falling film," J. Fluid Mech. **250**, 433 (1993).
[27] D. J. Benney, "Long waves on liquid films," J. Math. Phys. **45**, 150 (1966).
[28] S. P. Lin, "Finite amplitude side-band stability of a viscous film," J. Fluid Mech. **63**, 417 (1974).
[29] P. Rosenau and A. Oron, "Bounded and unbounded patterns of the Benney equation," Phys. Fluids A **4**, 1102 (1992).
[30] E. A. Demekhin, I. A. Demekhin, and V. Y. Shkadov, "Solitons in flowing layer of a viscous fluid," Izv. Akad. Nauk. SSSR, Mekh. Zhid. Gaza, No. 4, 9 (1983) [English translation: Fluid Dyn. **18**, 500 (1983)].
[31] T. Kawahara and S. Toh, "Pulse interactions in an unstable dissipative-dispersive nonlinear system," Phys. Fluids **31**, 2103 (1988).
[32] C. Elphick, G. R. Ierley, O. Regev, and E. A. Spiegel, "Interacting localized structures with Galilean invariance," Phys. Rev. A **44**, 1110 (1991).
[33] A. L. Frenkel, "Nonlinear theory of strongly undulating thin films flowing down a vertical cylinder," Europhys. Lett. **18**, 583 (1992).
[34] V. I. Kerchman and A. L. Frenkel, "Interactions of coherent structures in a film flow: simulations of a highly nonlinear evolution equation," Theoret. Comput. Fluid Dyn. (in press, 1994).
[35] D. Quéré, "Thin films flowing on vertical fibers," Europhys. Lett. **13**, 721 (1990).
[36] The measured linear velocity has the similar shape as the theoretical curve, but is 2%–5% larger. This small discrepancy has also been observed in previous work and was previously suggested to be a finite amplitude effect.
[37] B. Gjevik, "Spatially varying finite-amplitude wave trains on falling liquid films," Acta Polytech. Scand. Me **61**, 1 (1971).

[38]N. J. Zabusky and M. D. Kruskal, "Interaction of the 'solitons' in a collisionless plasma and the recurrence of initial states," Phys. Rev. Lett. **15**, 240 (1965).
[39]J. L. Hammack and D. M. Henderson, "Resonant interactions among surface water waves," Annu. Rev. Fluid Mech. **25**, 55 (1993).
[40]The synchronized interval appears to be 0.38 s instead of 0.40 s (the forcing period). This discrepancy is due to a small number of spurious noise pulses that are hard to eliminate in an automated measurement.